Optics & Laser Technology 202 (2026) 115435

Contents lists available at ScienceDirect

Optics and Laser Technology

journal homepage: www.elsevier.com/locate/optlastec

Full length article

Red diode-pumped alexandrite regenerative amplifier generating up to 78 μJ and down to 260 fs pulses

Tobias Grätzer, Manuel Zeyen, Markus Höck, Bojan Resan *

Photonic Ultrafast Systems Group, School of Engineering and Environment, University of Applied Sciences and Arts Northwestern Switzerland (FHNW), Switzerland

ARTICLE INFO

Keywords:
Ultrafast lasers
Red laser diode
Alexandrite
Femtosecond amplifiers
Regenerative amplifier

ABSTRACT

We present the first red diode-pumped alexandrite ultrafast amplifier, as well as the first red diode-pumped femtosecond alexandrite master oscillator power amplifier system. We achieved amplification of 90 fs pulses from nJ to μJ pulse energies and compression of the amplified pulses to 260 fs at 133 kHz, with a pulse energy of 2.5 μJ. A maximum pulse energy of 78 μJ is achieved at a repetition rate of 2 kHz. The amplifier output beam quality was good, with measured $M^2 = 1.35$.

1. Introduction

Femtosecond lasers with μJ pulse energies, emitting in the near-infrared (NIR) and ultraviolet (UV) regions, are needed in numerous micromachining applications, including consumer electronics [1], solar cell production [2], the fabrication of microfluidic devices [3], and biomedical cell surgery [4]. The laser gain medium alexandrite (Cr^{3+}:$BeAl_2O_4$) enables access to both NIR and UV, since its emission wavelength is centered around 755 nm, and can be converted efficiently to UV with second harmonic generation [5,6]. The large emission bandwidth of alexandrite spanning 700–850 nm, allows the generation of sub 20 fs pulses [7]. For many applications in the NIR, this pulse length is comparable to the output of Ti:Sapphire lasers and it is much shorter than the pulse durations typically available from Yb- or Nd-doped high-power modelocked lasers, with emission bandwidths of 10–20 nm. The opto-mechanical properties of alexandrite and the feature that its emission cross section increases with temperature [7,8] make it better suited than Ti:Sapphire for high-power ultrafast applications [9]. Furthermore, red laser diodes emitting around 638 nm can be used to pump alexandrite with a low quantum defect, which is a requirement for scaling up of average power. Therefore, red diode-pumped alexandrite lasers have attracted attention in recent years. In CW operation, 26.2 W average power with a slope efficiency of 49% has been achieved [10], while in Q-switched mode 3 mJ at 10 kHz repetition rate has been reported [11]. A thin-disk oscillator delivering 15 W in CW was recently demonstrated [12]. Mode-locking of a red-diode pumped alexandrite was first achieved with GHz pulse repetition rates and low pulse energies [13], then with a carbon nanotube saturable absorber [14] and subsequently, SESAM modelocking generating 100 fs pulses and Kerr-lens mode-locking, generating pulse durations as short as 44 fs were demonstrated [15].

As ultrafast oscillators typically deliver low pulse energies (pJ to nJ) [13,14], a high total gain of $> 10^3$ is required to achieve μJ pulse energies, needed for micromachining applications. While red diode-pumped and blue LED-pumped alexandrite oscillators and multi-pass amplifiers have been developed generating high energy pulses with nanosecond and microsecond duration [16–18], the total gain in these systems was limited due to the low small-signal gain of alexandrite [19] and the limited number of passes in the multi-pass amplifier architecture. Achieving large gain values is thus only feasible with regenerative amplifiers with many round-trips [20]. Low-repetition rate, flash-lamp-pumped and alexandrite-pumped ultrafast alexandrite regenerative amplifiers have been demonstrated achieving 10 mJ output pulse energy and $< 0.02\%$ optical-to-optical efficiency [21,22]. Most recently a nanosecond pulse red diode-pumped regenerative alexandrite amplifier delivering 1.1 mJ pulse energy at 1 kHz repetition rate was reported [23].

To the best of our knowledge, this work is the first demonstration of an ultrafast all red diode-pumped alexandrite master oscillator power amplifier (MOPA) system. We report the amplification of 90 fs pulses from our previously described red diode-pumped SESAM mode-locked alexandrite oscillator [15] by a factor of 10^5 to the μJ pulse energy level in a red diode-pumped alexandrite regenerative amplifier.

* Corresponding author.
E-mail address: bojan.resan@fhnw.ch (B. Resan).

https://doi.org/10.1016/j.optlastec.2026.115435
Received 13 March 2026; Received in revised form 18 April 2026; Accepted 29 April 2026
Available online 6 May 2026

2. Experimental setup

The MOPA system shown in Fig. 1 consists of a mode-locked alexandrite seed laser, mode-matching optics, a regenerative amplifier, and a grating compressor. The seed laser is the red diode-pumped SESAM mode-locked alexandrite laser described earlier [15]. The output of the oscillator is imaged onto the end mirror of the regenerative amplifier with a magnification of 0.7 using a telescope consisting of two plano-convex lenses, labeled L1 and L2. The separation of the seed input beam and the amplifier output beam is achieved with an optical isolator. A half-waveplate (WP1) is used to rotate the seed laser polarization to align it with the transmission axis of the isolator. The seed pulses pass through the thin-film polarizer (TFP) and are trapped in the amplifier by switching the Beta-Barium Borate (BBO) Pockels cell (Leysop BBO-3–25-AR750-DMP-NW) from 0 V to its quarter-wave voltage of ~ 2 kV. The amplified pulses are coupled out by switching the Pockels cell voltage back to 0 V. The optical resonator of the amplifier includes mirrors M1-M6, D1, D2, and the TFP. Mirrors M2, M3, and M5 are concave, with radii of curvature of 500 mm (M2 and M5) and 400 mm (M3). Mirrors D1 and D2 are dichroic, providing high transmission (>95%) at the pump wavelength and high reflectivity (>99.9%) at the laser emission wavelength. The eigenmode of the resonator has a beam waist of 140 μm ($1/e^2$) inside the alexandrite crystal and a beam waist of 250 μm ($1/e^2$) in the Pockels cell. The gain medium is a normal-incidence, anti-reflection-coated alexandrite crystal with a length of 7 mm and a doping concentration of 0.2 at. %, mounted in a temperature-controlled mount. The pump source is a fiber-delivered diode module emitting at 638 nm, with a fiber core diameter of 105 μm, a numerical aperture of 0.22, and a maximum output power of 8 W.

The fiber output is imaged through a plane dichroic mirror (D1) into the alexandrite crystal, using two groups of lenses with a magnification of 1.5. This lens system consists of an air-spaced doublet for collimation (F1) and an air-spaced triplet for focusing (F2). It achieves close to diffraction-limited performance (Strehl ratio > 0.9) at the pump wavelength. The pump beam waist is 75 μm (86% enclosed power fraction), has a beam quality factor of $M^2 = 35$, and a top-hat beam profile. The unpolarized pump light is only partially absorbed after a single pass through the crystal ($P_{abs} \approx 70\%$), due to strongly polarization-dependent absorption cross-section of alexandrite [7]. To improve the absorption, a double-pass pump system was added, consisting of a second dichroic mirror (D2), an aspherical lens (f = 100 mm), a quarter-wave plate (WP2), and a highly reflective mirror. The unabsorbed pump light is collimated by the aspheric lens, and its polarization is rotated by 90° via a double pass through the quarter-wave plate. This aligns the polarization of the reflected light with the highly absorbing b-axis of the alexandrite crystal, resulting in ~ 90% total pump absorption efficiency.

The number of round-trips in the regenerative cavity needed to reach the desired total gain is relatively high (~450), which stretches the seed pulses to ~ 70 ps due to material dispersion introduced by the Pockels cell and the alexandrite crystal. This eliminates the need for a separate stretcher at the amplifier input to prevent excessively high peak powers. The stretched output pulses from the amplifier are compressed in a Treacy-style grating compressor, which uses a single transmission grating (1380 lines/mm) set at the Littrow angle, along with two roof mirrors that fold the beam path and spatially recombine the dispersed beam.

3. Results

3.1. Oscillator

The SESAM mode-locked seed laser emits fs pulses with a pulse energy of 1.2 nJ at a repetition rate of 84 MHz. As shown in Fig. 2(a), the optical spectrum is centered at 745 nm with a full width at half maximum (FWHM) of 8 nm. The autocorrelation measurement in Fig. 2 (b) demonstrates the pulse duration of 90 fs (assuming a sech2 temporal pulse shape). With a time-bandwidth product of 0.388, the pulses are close to transform-limited. The radio-frequency spectrum has a signal-to-noise ratio of 75 dB at a span of 1 MHz and a resolution bandwidth of 100 Hz [15], indicating low-noise mode-locked operation. The

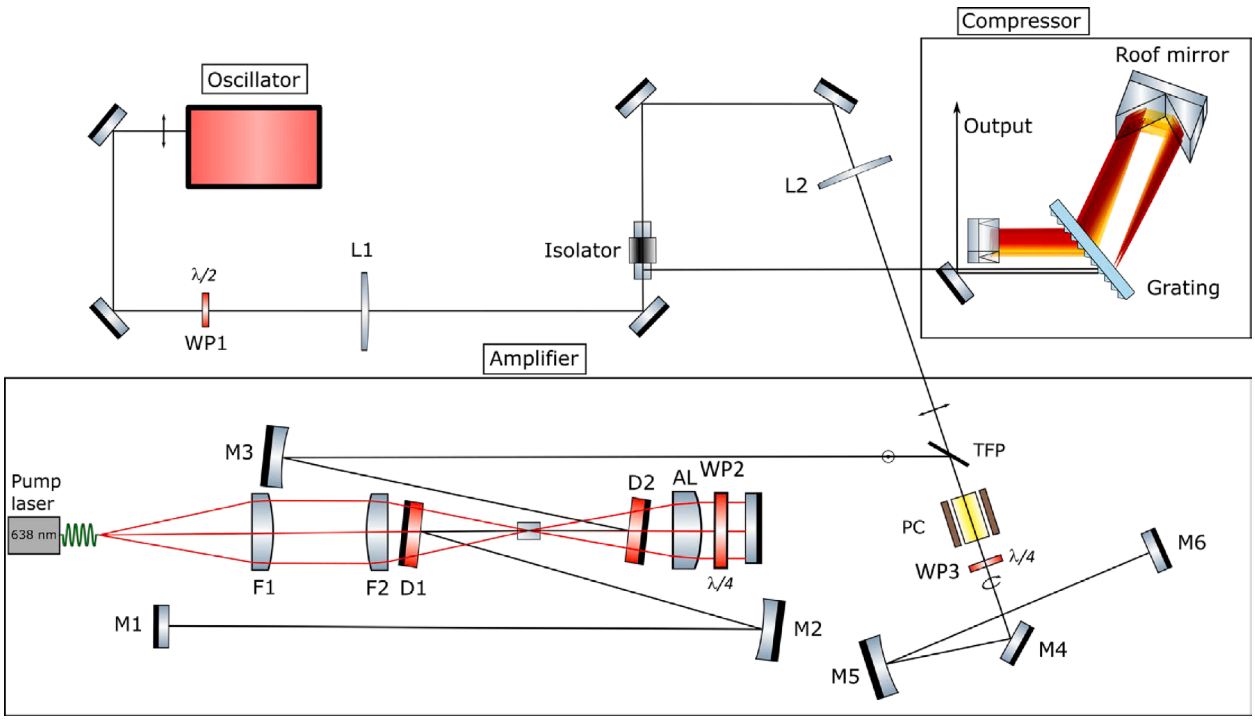

Fig. 1. Schematic of the ultrafast red diode-pumped alexandrite Master Oscillator Power Amplifier system: TFP: thin-film polarizer, PC: Pockels cell, D1: dichroic mirror 1, D2: dichroic mirror 2, AL: aspheric lens, M1-6: high reflection mirrors, WP1: half- wave plate, WP2,3: quarter-wave plates, F1: lens group 1, F2: lens group 2.

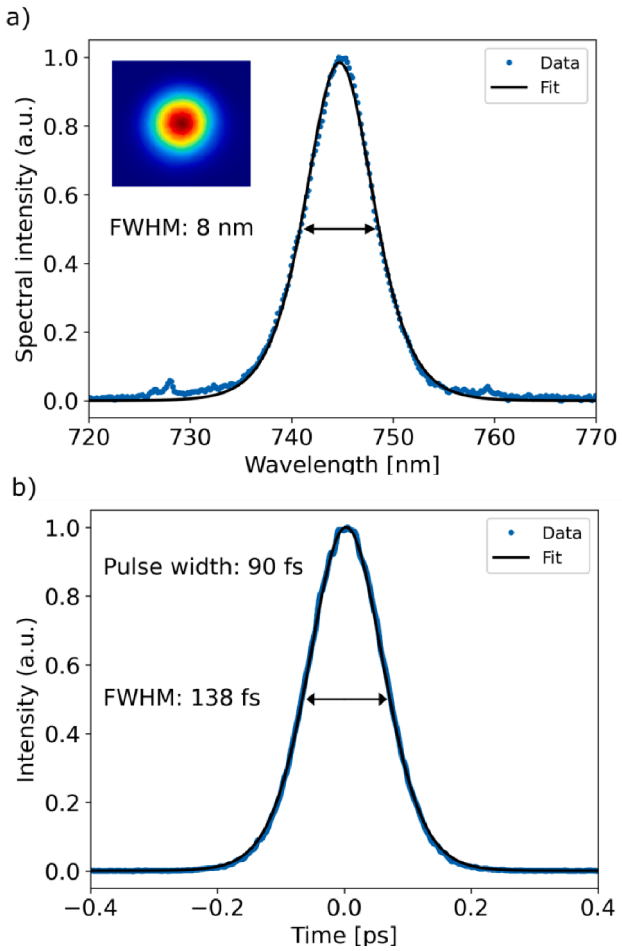

Fig. 2. A) Measured optical spectrum of the seed pulses. The fit is a sech2 function. The inset image shows the seed beam profile. **b)** Measured autocorrelation trace of the seed pulses. The fit is a $sech^2$ function.

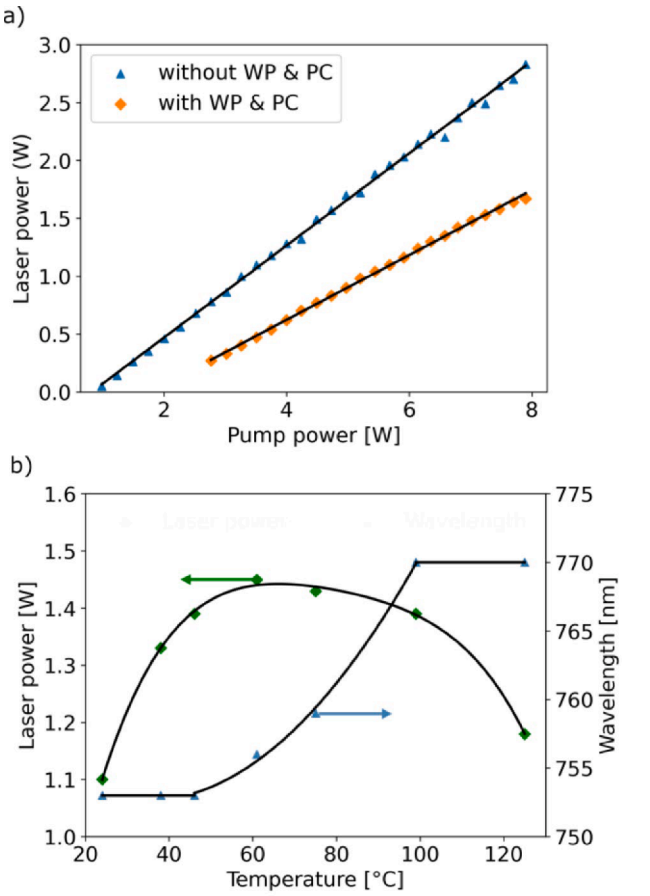

Fig. 3. A) Output power versus pump power for the amplifier operated as a free-running CW oscillator with and without the Pockels cell (PC) and waveplate (WP). **b)** Output power and emission wavelength versus crystal temperature without the Pockels cell present, using the waveplate and TFP as a variable output coupler.

output has a beam quality of $M^2 = 1.15$. The image inset in Fig. 2(a) shows the corresponding Gaussian output beam profile.

3.2. Amplifier in CW operation

The performance of the amplifier as a free-running CW oscillator, is assessed with and without the Pockels cell and waveplate WP3 in the cavity. The resonator without the Pockels cell and quarter-wave plate produces a maximum output power of 2.8 W at a pump power of 7.9 W, as shown in Fig. 3(a), using an output coupler with 1% transmission. This results in an optical-to-optical efficiency of 36% with a slope efficiency of 40%. The output beam has excellent beam quality ($M_x^2 = 1.2$, $M_y^2 = 1.15$). When the Pockels cell and quarter-wave plate are added to the cavity, the output coupler is replaced with an HR mirror. The waveplate WP3 and TFP are used as a variable output coupler, with the waveplate angle adjusted to maximize output power through the TFP. The output power achieved in this configuration is 1.67 W at a pump power of 7.9 W, corresponding to an optical-to-optical efficiency of 21% with a slope efficiency of 27%. The reduced output power and efficiency are due to additional losses from the AR-coated Pockels cell and the waveplate. The dependence of output power and emission wavelength on the alexandrite crystal temperature is shown in Fig. 3(b). In these measurements, the Pockels cell is not included in the resonator, keeping only the TFP and the waveplate as a variable output coupler so that the output power is maximized for each temperature by tuning the waveplate angle. The emission wavelength is tunable from 753 nm to 770 nm by varying the crystal temperature from 60 °C to 100 °C, with a slight reduction in output power at higher temperatures. Variations of the crystal temperature did not significantly affect the pump absorption, which is also in accordance with work published elsewhere [24]. The TFP exhibits a drop in reflectivity above 770 nm, which likely limits its tunability at longer wavelengths. While the output power is significantly reduced below 45 °C, power fluctuations at lower temperatures are also reduced. Therefore, a crystal temperature of 45 °C is selected as a compromise between output power and stability.

3.3. Amplification of seed pulses

The seed pulses, with an energy of 0.6 nJ and a pulse repetition rate of 84 MHz (measured before the TFP), are amplified over 448 round-trips to reach a pulse energy of 3 μJ at a repetition rate of 133 kHz and a pump power of 7.5 W. This corresponds to a total gain of 37 dB. Fig. 4(a) shows the exponential growth of intracavity pulse energy within the amplifier, measured with a fast photodiode located behind an end mirror. A round-trip small-signal gain of 2% is inferred from the pulse energy growth, which shows no signs of gain saturation. The output of the amplifier is stigmatic, with a beam quality of $M_x^2 = 1.39$ and $M_y^2 = 1.31$. The image inset in Fig. 4(a) displays the beam profile of the amplifier measured behind an end mirror.

In the present setup, the measured beam profile includes contributions from the seed beam passing through the amplifier during the pump phase. As the pump-induced lens in the crystal distorts the wavefront of the seed beam, the beam quality degrades. This wavefront distortion appears as a weak concentric ring around the central peak in the beam

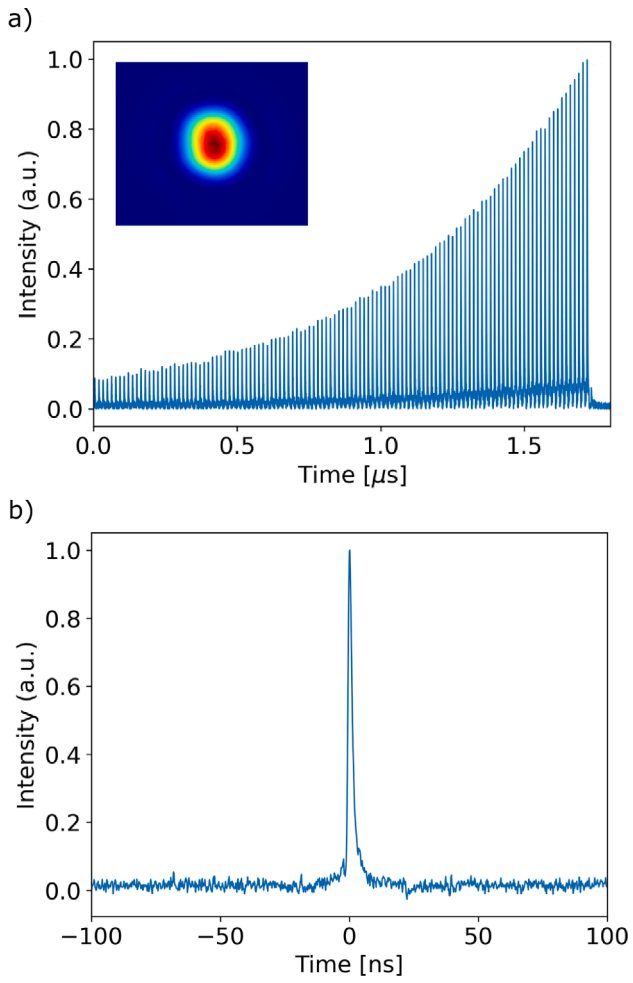

Fig. 4. A) Measured intracavity pulse build-up with inset beam profile at 133 kHz repetition rate. **b)** Time trace of a typical output pulse at 133 kHz repetition rate.

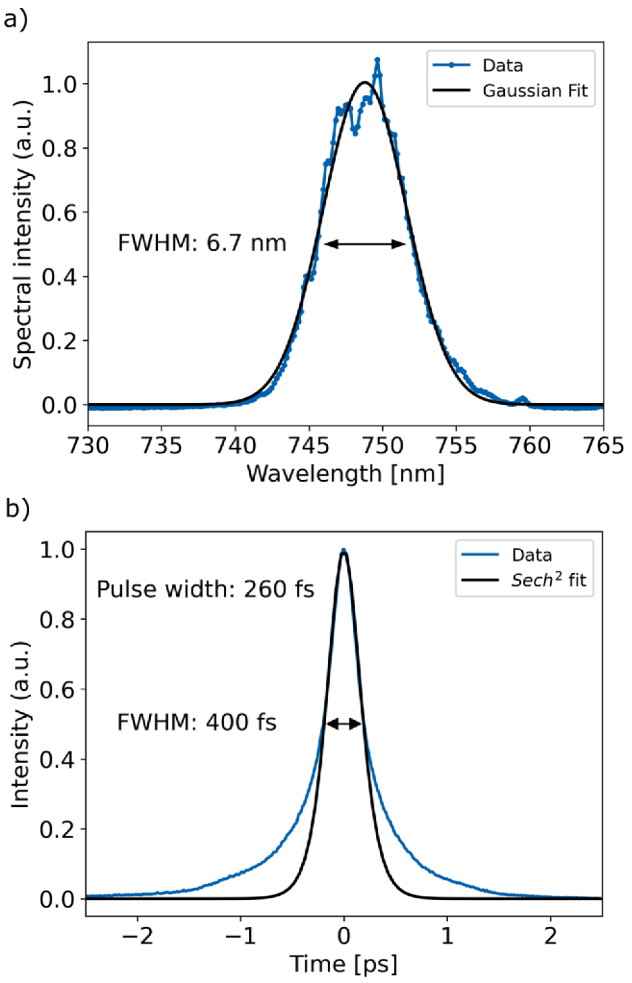

Fig. 5. A) Measured optical spectrum of the amplified pulses at 133 kHz repetition rate. **b)** Autocorrelation measurement of the compressed pulses at 133 kHz repetition rate.

profile. The beam quality of the amplified pulses, excluding the wavefront error contribution from the seed beam, is expected to be closer to that achieved in CW operation ($M^2 \approx 1.2$). The output pulse train consisted of stable amplified pulses at the trigger frequency of the Pockels cell. Fig. 4(b) shows the output pulse on a timescale approximately 10 times the cavity round-trip time (14.7 ns), demonstrating a clean, single pulse with negligible pre- and post-pulses.

As shown in Fig. 5(a), the center wavelength of the amplified pulses is 749 nm, and the FWHM is 6.7 nm. The spectrum is shifted towards longer wavelengths, consistent with the gain peak of the amplifier at 753 nm when operated in CW (see Fig. 3(b)). The narrowing of the spectrum is caused by gain-narrowing effects originating from the finite bandwidths of the gain medium and the intracavity elements. Fig. 5(b) shows the autocorrelation trace of the compressed pulses with a pulse duration of 260 fs, assuming a sech^2 pulse shape. Compared to the sech^2 fit, additional 'wings' are visible in the autocorrelation trace, which are characteristic of uncompensated third-order dispersion (TOD). Both the amplifier and the compressor introduce significant third-order dispersion. This results in additional post-pulse ripples. Thus, the pulse duration of 260 fs is an estimate of the pulse duration of the main pulse. The compressor achieves an optical efficiency of 83%, resulting in output compressed pulses with a pulse energy of 2.5 μJ.

The contribution of amplified spontaneous emission (ASE) is assessed by comparing the average output power of the amplifier in unseeded and seeded modes (blocking or transmitting the seed beam to the amplifier). Based on this measurement, approximately 3% of the total pulse energy is attributed to ASE at this repetition rate. This results in an intensity contrast between ASE and the main pulse of $\sim 10^6$ after compression.

The amplifier is designed to operate at high repetition rates and moderate pulse energies. However, to demonstrate the capability of the system to achieve much higher pulse energies, operation at 2 kHz repetition rate is investigated. A maximum pulse energy of 78 μJ and a total gain of 51 dB is achieved after 430 round-trips. Under these conditions, the gain is fully saturated, as shown in Fig. 6(a), which illustrates the growth of the intracavity pulse energy. The small-signal gain per round trip is 2.7%. The pulse duration after compression is around 700 fs at these high pulse energies. The low repetition rate resulted in undersampling of the autocorrelation trace, preventing an accurate measurement. Qualitatively, the longer pulse duration results from the accumulated cubic spectral phase due to stronger self-phase modulation (for high energy, low repetition rate operation) and TOD in the amplifier and compressor, which will be explained in detail in the discussion section.

The optical spectrum has a FWHM of 6.9 nm, centered at 749 nm, as shown in Fig. 6(b). The absence of further spectral narrowing compared to amplification at lower pulse energies, as shown above, indicates that gain narrowing is offset by spectral broadening due to self-phase modulation. The measured pulse-to-pulse energy fluctuation is around 2.5% rms, measured over 50′000 pulses.

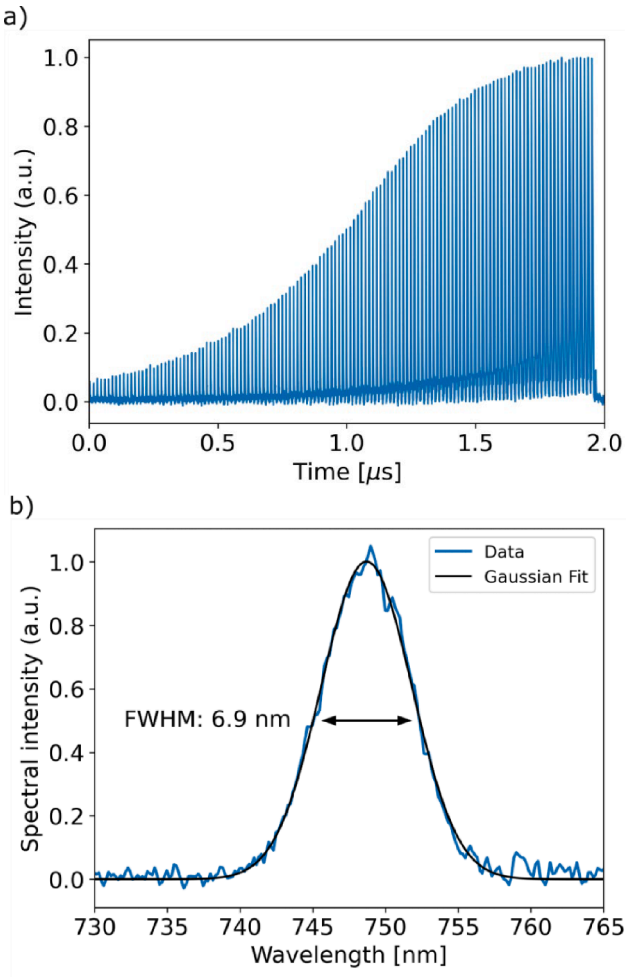

Fig. 6. A) Measured intracavity pulse build-up at 2 kHz repetition rate and 78 μJ output pulse energy. **b)** Measured optical spectrum of the output pulses at 2 kHz repetition rate.

4. Discussion

The amplification efficiency of any regenerative amplifier is heavily affected by the ratio of small-signal gain to intracavity losses. The diameter of the pump beam was optimized with a simple geometrical model that maximized the average small signal gain over the length of the crystal for a given laser mode size. The small signal gain along the crystal axis was calculated by considering the exponential absorption of the pump light along the axis, and the high divergence of the pump beam (obtained from its high M^2 value). For our set of parameters, a diameter of the pump beam in the focus of approximately 80 μm, located close to the input surface of the alexandrite crystal, yielded the best results. We optimized the pump beam imaging system, to preserve pump brightness and to maximize gain by fine-tuning the pump spot diameter. To reduce amplifier losses, a BBO Pockels cell without additional protective windows was used. The seed laser emits at an 8 nm shorter wavelength (745 nm) than the gain peak of the amplifier (753 nm), resulting in reduced gain and stronger gain narrowing. The wavelength mismatch is due to the SESAM used to modelock the oscillator, which is centered at 740 nm. When operated as a free-running oscillator, the amplifier could be tuned from 753 nm to 770 nm by varying the crystal temperature. Shorter wavelengths were not accessible due to coating limitations of the optical components of the regenerative cavity. Therefore, the wavelength of the seed laser should be matched closer to the gain peak of the amplifier, by optimizing the SESAM, or by using a broader bandwidth Kerr-lens modelocked oscillator, which would also deliver shorter pulse durations, as demonstrated previously [15].

As shown in Fig. 4(a), we do not reach gain saturation at the higher pulse repetition rate of 133 kHz in 448 round-trips. However, if the number of round-trips was increased at 133 kHz pulse repetition rate, a significant degradation in the pulse contrast was detected. If the number of round trips is increased further, the amplifier starts lasing in CW mode when it is not seeded and there may be a significant CW background below femtosecond pulses when it is seeded.

The amplifier output was unstable in a small window of repetition rates between 5–10 kHz. We attribute this instability to strong coupling between the inversion and the intracavity photon population on time scales where the upper state lifetime and the round-trip time of the regenerative amplifier approximately match [25]. At lower or higher repetition rates, however, we did not observe any instabilities. This is due to the fact that the laser ions in the alexandrite crystal are directly pumped into the upper laser level when pumping with red light, so that the coupling between phonons and the excited state population is suppressed, which has been shown to be the leading cause of chaotic pulsing in alexandrite lasers [26,27].

At moderate pulse energies, the pulse compression is limited to roughly three times the transform limit by residual TOD. The contributions of the amplifier (1.38×10^6 fs^3) and the compressor (4.65×10^6 fs^3) are calculated according to [28] yielding a total residual TOD of 6×10^6 fs^3. The primary source of TOD is the grating compressor, which introduces positive TOD and negative group delay dispersion (GDD), to compensate for positive GDD introduced by the amplifier. The number of round-trips not only affects the GDD and TOD introduced by the amplifier but also the TOD introduced by the compressor. This is because GDD and TOD introduced by the compressor are proportional to each other, with their ratio depending on wavelength, grating periodicity, and grating angle. Fewer round-trips result in less GDD from the amplifier and, consequently, less GDD and TOD from the compressor.

Reducing the number of round-trips from 450 to 350 improved pulse compression to ~ 200 fs but also reduced the output pulse energy. Improved pulse compression without sacrificing pulse energy may be achievable by increasing the small-signal gain, seed pulse energy, or seeding efficiency, thereby achieving the same total gain with fewer round-trips. Further improvements in pulse compression to ~ 160 fs were achieved by additional clipping of the spatially dispersed beam in the compressor, thereby reducing the spectral width and the impact of TOD on the pulse compression, but also further reducing the pulse energy. Dispersion compensation up to the third order and thus significantly shorter pulses could be achieved by adding specially designed chirped mirrors with negative TOD to the amplifier cavity to counteract the TOD of the intracavity elements and precompensate for the compressor's TOD.

In the future, it should be feasible to reduce the pulse length of the amplifier output to around 30 fs, to reach a comparable performance level to the state-of-the-art Ti:sapphire amplifiers. At 750 nm central wavelength, such pulses require a spectral bandwidth of > 20 nm. Assuming an amplification factor of 1000, the input pulse must have approximately twice the bandwidth to counteract the gain narrowing during the amplification process. We already achieved seed pulses with spectral bandwidth of 19 nm from a Kerr-lens mode locked red diode-pumped alexandrite oscillator [15], and our future work will focus on achieving seed pulses with > 50 nm bandwidth. The alexandrite medium theoretically supports such a bandwidth, and it should be reachable using standard pulse shaping methods.

5. Conclusion

We demonstrate, to the best of our knowledge, the first ultrafast diode-pumped alexandrite amplifier and an ultrafast diode-pumped alexandrite master oscillator power amplifier (MOPA) system. We report the amplification of sub-100 fs pulses with 0.6 nJ pulse energy to 78 μJ at a 2 kHz pulse repetition rate, and pulse compression to 260 fs

with 2.5 μJ pulse energy at 133 kHz repetition rate, in a red diode-pumped alexandrite regenerative amplifier. Due to low quantum-defect pumping and high performance at elevated crystal temperatures, there is significant potential to scale the output power of red diode-pumped alexandrite lasers. We plan to increase the system's average power to the multi-Watt level by increasing the pump power, repetition rate, and optimized seeding. In this work, pulse compression was limited by residual third-order dispersion. We aim to reduce the output pulse duration of the amplifier to below 100 fs, using shorter seed pulse duration and improving third-order dispersion compensation. Red diode-pumped femtosecond alexandrite amplifiers are promising for demanding micromachining applications in IR and UV spectral regions.

CRediT authorship contribution statement

Tobias Grätzer: Writing – review & editing, Writing – original draft, Visualization, Validation, Methodology, Investigation, Formal analysis, Data curation, Conceptualization. **Manuel Zeyen:** Writing – review & editing, Visualization, Validation, Supervision, Software, Methodology, Investigation, Formal analysis, Data curation. **Markus Höck:** Writing – review & editing, Investigation, Data curation, Formal analysis, Methodology, Validation. **Bojan Resan:** Writing – review & editing, Validation, Supervision, Resources, Project administration, Methodology, Funding acquisition, Conceptualization, Formal analysis, Investigation.

Funding

This project is partially funded by Swiss Nanoscience Institute, project Diffractive Optics.

Declaration of competing interest

The authors declare that they have no known competing financial interests or personal relationships that could have appeared to influence the work reported in this paper.

Data availability

Data will be made available on request.

References

[1] S. Ahn, J. Kim, D. Lee, et al., Enhancement of electrical conductivity during the femtosecond laser trimming process for OLED repair, Opt. Lasers Eng. 137 (2021) 106381, https://doi.org/10.1016/j.optlaseng.2020.106381.
[2] J. Hermann, M. Benfarah, S. Bruneau, et al., Comparative investigation of solar cell thin film processing using nanosecond and femtosecond lasers, J. Phys. D Appl. Phys. 39 (3) (2006) 453, https://doi.org/10.1088/0022-3727/39/3/005.
[3] F. Sima, K. Sugioka, R. Martínez Vázquez, et al., Three-dimensional femtosecond laser processing for lab-on-a-chip applications, Nanophotonics 7 (3) (2018) 613–634, https://doi.org/10.1515/nanoph-2017-0097.
[4] G.J. Tserevelakis, S. Psycharakis, B. Resan, et al., Femtosecond laser nanosurgery of sub-cellular structures in HeLa cells by employing third harmonic generation imaging modality as diagnostic tool, J. Biophotonics 5 (2) (2012) 200–207, https://doi.org/10.1002/jbio.201100055.
[5] M. Liang, A. Minassian, M.J. Damzen, High-energy acousto-optic Q-switched alexandrite laser with wavelength tunable fundamental and UV second harmonic generation, Opt Express OE 31 (25) (2023) 42428–42438, https://doi.org/10.1364/OE.505385.
[6] H. Xiao, A.-H. Munj, A. Minassian, et al., High-efficiency deep-UV output from a diode-pumped alexandrite laser, Opt Express OE 33 (19) (2025) 39229–39237, https://doi.org/10.1364/OE.571272.
[7] U. Demirbas, A. Sennaroglu, F.X. Kärtner, Temperature dependence of Alexandrite effective emission cross section and small signal gain over the 25-450 °C range, Opt. Mater. Express 9 (8) (2019) 3352–3370, https://doi.org/10.1364/OME.9.003352.
[8] J. Walling, O. Peterson, H. Jenssen, et al., Tunable alexandrite lasers, IEEE J. Quantum Electron. 16 (12) (1980) 1302–1315, https://doi.org/10.1109/JQE.1980.1070430.
[9] U. Demirbas, F.X. Kärtner, Alexandrite: an attractive thin-disk laser material alternative to Yb:YAG? J. Opt. Soc. Am. B 37 (2) (2020) 459–472, https://doi.org/10.1364/JOSAB.380140.
[10] A. Teppitaksak, A. Minassian, G.M. Thomas, et al., High efficiency >26 W diode end-pumped Alexandrite laser, Opt Express, OE 22 (13) (2014) 16386–16392, https://doi.org/10.1364/OE.22.016386.
[11] G.M. Thomas, A. Minassian, X. Sheng, et al., Diode-pumped Alexandrite lasers in Q-switched and cavity-dumped Q-switched operation, Opt Express OE 24 (24) (2016) 27212–27224, https://doi.org/10.1364/OE.24.027212.
[12] M. Ghawas, T. Graf, M.A. Ahmed, Continuous-wave alexandrite thin-disk laser in multi-mode and fundamental-mode operation, Opt. Continuum 5 (2) (2026) 379–388, https://doi.org/10.1364/OPTCON.587568.
[13] R. Miao, Y. Nie, S. Wang, et al., Self-mode-locked alexandrite femtosecond lasers with multi-GHz repetition rates, Opt. Lett. 46 (8) (2021) 1979–1982, https://doi.org/10.1364/OL.423249.
[14] E. Cai, S. Zhang, M. Jiang, et al., 638-nm laser-diode pumped alexandrite femtosecond laser passively mode-locked by single-walled carbon nanotubes, Opt. Express 32 (14) (2024) 25463–25471, https://doi.org/10.1364/OE.529959.
[15] T. Grätzer, M. Zeyen, D. Hug, et al., Red diode-pumped SESAM and Kerr-lens modelocked alexandrite lasers, Opt Express OE 32 (26) (2024) 47033–47040, https://doi.org/10.1364/OE.542834.
[16] P. Pichon, A. Barbet, J.-P. Blanchot, et al., LED-pumped alexandrite laser oscillator and amplifier, Opt. Lett. OL 42 (20) (2017) 4191–4194, https://doi.org/10.1364/OL.42.004191.
[17] A.T. Coney, M.J. Damzen, High-energy diode-pumped alexandrite amplifier development with applications in satellite-based lidar, J. Opt. Soc. Am. B 38 (1) (2021) 209, https://doi.org/10.1364/JOSAB.409921.
[18] E. Thellier, H. Taleb, F. Druon, et al., LED pumped alexandrite multipass amplifier designed for acousto-optic imaging, Opt Express OE 33 (19) (2025) 40727–40738, https://doi.org/10.1364/OE.563688.
[19] E. Beyatli, I. Baali, B. Sumpf, et al., Tapered diode-pumped continuous-wave alexandrite laser, J. Opt. Soc. Am. b, JOSAB 30 (12) (2013) 3184–3192, https://doi.org/10.1364/JOSAB.30.003184.
[20] S. Biswal, J. Itatani, J. Nees, et al., Efficient energy extraction below the saturation fluence in a low-gain low-loss regenerative chirped-pulse amplifier, IEEE J. Sel. Top. Quantum Electron. 4 (2) (1998) 421–425, https://doi.org/10.1109/2944.686750.
[21] D.J. Harter, P. Bado, Wavelength tunable alexandrite regenerative amplifier, Appl. Opt. 27 (21) (1988) 4392–4395, https://doi.org/10.1364/AO.27.004392.
[22] A. Hariharan, M.E. Fermann, M.L. Stock, et al., Alexandrite-pumped alexandrite regenerative amplifier for femtosecond pulse amplification, Opt. Lett. OL 21 (2) (1996) 128–130, https://doi.org/10.1364/OL.21.000128.
[23] J. Wang, S. Sun, S. Wang, et al., Revisiting Alexandrite regenerative amplifier (Alex-RA) after 3 decades: first demonstration of LD-pumped Alex-RA at 1 kHz repetition rate, Opt. Laser Technol. 193 (2026) 114205, https://doi.org/10.1016/j.optlastec.2025.114205.
[24] M. Fibrich, J. Šulc, D. Vyhlídal, et al., Alexandrite spectroscopic and laser characteristic investigation within a 78–400 K temperature range, Laser Phys. 27 (11) (2017) 115801, https://doi.org/10.1088/1555-6611/aa884c.
[25] J. Dörring, A. Killi, U. Morgner, et al., Period doubling and deterministic chaos in continuously pumped regenerative amplifiers, Opt Express OE 12 (8) (2004) 1759–1768, https://doi.org/10.1364/OPEX.12.001759.
[26] W. Gadomski, B. Ratajska-Gadomska, Homoclinic orbits and chaos in the vibronic short-cavity standing-wave alexandrite laser, J. Opt. Soc. Am. B 17 (2) (2000) 188, https://doi.org/10.1364/JOSAB.17.000188.
[27] H. Ogilvy, M.J. Withford, R.P. Mildren, et al., Investigation of the pump wavelength influence on pulsed laser pumped Alexandrite lasers, Appl. Phys. B 81 (5) (2005) 637–644, https://doi.org/10.1007/s00340-005-1948-5.
[28] S. Backus, C.G. Durfee, M.M. Murnane, et al., High power ultrafast lasers, Rev. Sci. Instrum. 69 (3) (1998) 1207–1223, https://doi.org/10.1063/1.1148795.